





Article

Plumbogaidonnayite, $\text{PbZrSi}_3\text{O}_9 \cdot 2\text{H}_2\text{O}$, a new Pb-member of the gaidonnayite group from the Saima alkaline complex, Liaoning Province, China

Bin Wu¹ , Xiangping Gu² , Xin Gui¹, Christophe Bonnetti^{1,3}, Can Rao⁴, Rucheng Wang⁵, Jianjun Wan¹ and Wenlei Song⁶

¹State Key Laboratory of Nuclear Resources and Environment, East China University of Technology, Nanchang, Jiangxi 330013, China; ²School of Geosciences and Info-physics, Central South University, Changsha, Hunan 410083, China; ³Arethuse Geology EURL, 29 Allée de Saint Jean, Fuveau 13710, France; ⁴School of Earth Sciences, Zhejiang University, Hangzhou, Zhejiang 310027, China; ⁵State Key Laboratory for Mineral Deposits Research, School of Earth Sciences and Engineering, Nanjing University, Nanjing, Jiangsu 210033, China; and ⁶State Key Laboratory of Continental Dynamics, Department of Geology, Northwest University, Xi'an, Shaanxi 710069, China

Abstract

Plumbogaidonnayite, ideally $\text{PbZrSi}_3\text{O}_9 \cdot 2\text{H}_2\text{O}$, is a new gaidonnayite-group mineral discovered as a secondary product derived from the alteration of eudialyte from the Saima alkaline complex, China. It occurs as aggregates (up to 1 mm) composed of subhedral to anhedral or platy crystals (individually 5–50 μm), associated closely with microcline, natrolite, aegirine, gaidonnayite, georgechaoite, zircon, bob-trillite and britholite-(Ce) in eudialyte pseudomorphs. The crystals are transparent, colourless or light brown with a vitreous lustre. Plumbogaidonnayite is brittle with conchoidal fracture, and it has a Mohs hardness of ~ 5 and a calculated density of 3.264 g/cm^3 . It is optically biaxial (+) with $\alpha = 1.61(3)$, $\beta = 1.63(3)$ and $\gamma = 1.66(4)$. The calculated $2V$ is 80° , with the optical orientations X , Y and Z parallel to the crystallographic a , b and c axes, respectively. The empirical formula is $(\text{Pb}_{0.70}\text{Ca}_{0.17}\text{Ba}_{0.01}\text{K}_{0.11}\text{Na}_{0.01}\text{Y}_{0.01})_{\Sigma 1.01}(\text{Zr}_{1.00}\text{Hf}_{0.01}\text{Ti}_{0.01})_{\Sigma 1.02}\text{Si}_{3.01}\text{O}_9 \cdot 2\text{H}_2\text{O}$ calculated on the basis of nine oxygen atoms per formula unit and assuming the occurrence of two H_2O groups. Plumbogaidonnayite is orthorhombic, $P2_1nb$, $a = 11.7690(4) \text{ \AA}$, $b = 12.9867(3) \text{ \AA}$, $c = 6.66165(16) \text{ \AA}$, $V = 1018.17(5) \text{ \AA}^3$ and $Z = 4$. The nine strongest lines of its powder XRD pattern [d in Å (I , %) (hkl)] are: 6.489 (36) (020), 5.803 (100) (101), 4.661 (27) (021), 4.336 (29) (121), 3.640 (30) (221), 3.114 (79) (112), 2.947 (27) (400), 2.622 (27) (241) and 2.493 (27) (312). Plumbogaidonnayite has a similar spiral chain framework structure with gaidonnayite and georgechaoite, which is composed of SiO_4 tetrahedra and ZrO_6 octahedra, but with disordered extra-framework sites (cations and H_2O groups) characterised by the substitution of $2\text{Na}^+ (\text{K}^+) \rightarrow \text{Pb}^{2+} (\text{Ca}^{2+}) + \square$ (vacancy). The discovery of plumbogaidonnayite adds a new perspective on the cation ordering and heterovalent substitution mechanism in gaidonnayite-group minerals.

Keywords: plumbogaidonnayite; new mineral; chain silicate mineral; microporous zirconosilicate; Saima alkaline complex

(Received 2 August 2023; accepted 9 January 2024; Accepted Manuscript published online: 18 January 2024; Associate Editor: Anthony R Kampf)

Introduction

Microporous materials with zeolitic structure, specifically titanate and zirconosilicates with complex octahedral–tetrahedral frameworks, have been studied extensively owing to their industrial properties (e.g. ion-exchange, sorption and catalysis) in modern technologies (Mumpton, 1999; Kuznicki *et al.*, 2001; Celestian *et al.*, 2019). Gaidonnayite-group minerals are hydrous zirconosilicates with a microporous heteropolyhedral framework, though only two natural types of alkali metal-dominant members, namely gaidonnayite ($\text{Na}_2\text{ZrSi}_3\text{O}_9 \cdot 2\text{H}_2\text{O}$) and georgechaoite ($\text{KNaZrSi}_3\text{O}_9 \cdot 2\text{H}_2\text{O}$), have been reported (Chao and Watkinson, 1974; Boggs and Ghose, 1985).

The new mineral plumbogaidonnayite $\text{PbZrSi}_3\text{O}_9 \cdot 2\text{H}_2\text{O}$, the first divalent cation-dominant Pb member of the gaidonnayite group, was discovered in lujavrite from the Saima alkaline complex, Liaoning Province, China. This complex is also the type locality for fengchengite (IMA2007-018a), hezuolinite (IMA2010-045), and recently approved fluorsigaiite (IMA2021-87a) and gysinite-(La) (IMA2022-008, Yang *et al.*, 2012; Shen *et al.*, 2017; Wu *et al.*, 2022, 2023a). The prefix ‘plumbo’ was added to indicate its Pb-dominant compositional signature on the suggestion of the Commission on New Minerals, Nomenclature and Classification of the International Mineralogical Association (IMA–CNMNC, Hatert and Burke, 2008). This new species with the official name plumbogaidonnayite and symbol ‘Pgdn’ has been approved by the IMA–CNMNC (IMA2022-095, Wu *et al.*, 2023b). The type material (catalogue number M16139) has been deposited at the Geological Museum of China (No. 15 Yangrouhutong, Xisi, Beijing 100031, China). This paper presents the mineral paragenesis, chemical composition and crystal structure of plumbogaidonnayite,

Corresponding author: Bin Wu; Email: wubin@ecut.edu.cn

Cite this article: Wu B., Gu X., Gui X., Bonnetti C., Rao C., Wang R., Wan J. and Song W. (2024) Plumbogaidonnayite, $\text{PbZrSi}_3\text{O}_9 \cdot 2\text{H}_2\text{O}$, a new Pb-member of the gaidonnayite group from the Saima alkaline complex, Liaoning Province, China. *Mineralogical Magazine* 88, 185–194. <https://doi.org/10.1180/mgm.2024.2>

and compares its characteristics with other members of the gaidonnayite group.

Occurrence and origin

The Triassic Saima complex (220–230 Ma) is situated on the Liaodong Peninsula within the northeastern margin of the North China Craton, and within it lujavrite hosts typical alkaline rock-type Zr–REE–Nb mineralisation (where REE = rare earth elements, Wu *et al.*, 2016; Ma and Liu, 2023). The lujavrite, with ~20% exposed area, intruded the main body of nepheline syenite as sheets, stocks or dykes at the northeast and northwest edges of the complex. It is composed of predominantly K-feldspar, nepheline, aegirine, and variable amounts of Zr–REE–Nb-bearing accessory minerals including zircon, eudialyte, pyrochlore, rinkite-(Ce) and wadeite (Wu *et al.*, 2016). Late metasomatism such as alkali-metasomatism, skarnification and carbonation prevailed through the whole Saima alkaline complex

and led to the dissolution of precursor Zr–REE–Nb-bearing minerals (e.g. wadeite and eudialyte), and the precipitation of a series of secondary alteration minerals (e.g. natrolite, calcite, britholite-(Ce) and zircon, Wu *et al.*, 2015, 2018). The geological, mineralogical and geochronological features of the Saima complex have been reported extensively in recent work (e.g. Wu *et al.*, 2010, 2016; Zhu *et al.*, 2016, 2017).

Plumbogaidonnayite occurs as subhedral to anhedral or platy crystals of ~5–50 μm across, commonly forming aggregates (up to 1 mm) in pseudomorphs of altered eudialyte in Saima lujavrite (Fig. 1). It is associated closely with other secondary products after eudialyte alteration, including natrolite, aegirine, gaidonnayite, georgechaoite, zircon, bobtrillite and britholite-(Ce). Plumbogaidonnayite might be crystallised directly from eudialyte alteration, or, more likely, transformed from gaidonnayite or georgechaoite, which occur as the intermediate products after eudialyte alteration by the natural ion exchange $2\text{Na}^+(\text{K}^+) \rightarrow \text{Pb}^{2+}(\text{Ca}^{2+}) + \square$ (vacancy) as reported in other microporous framework

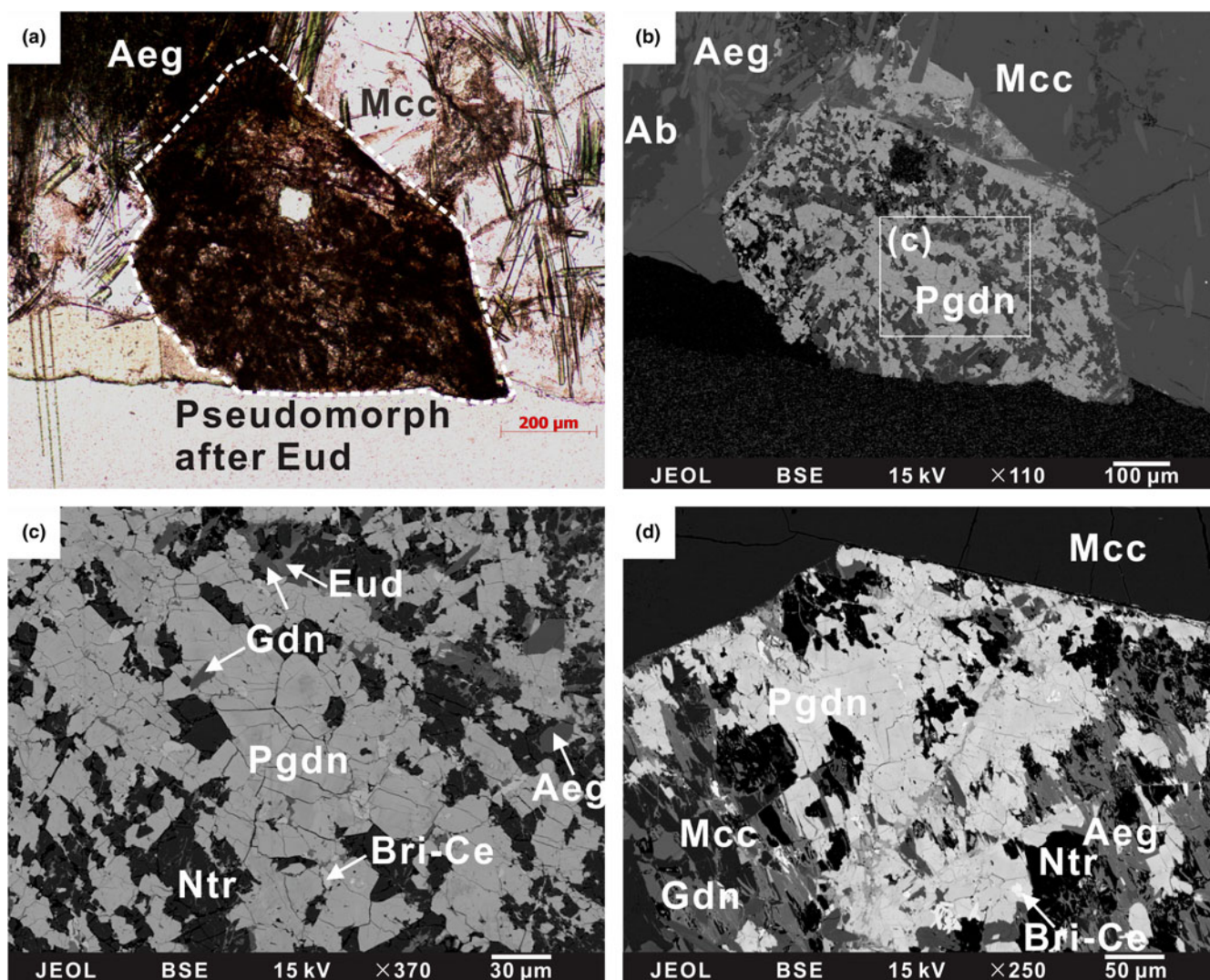


Figure 1. Photomicrograph (a) and back-scattered electron images (b–d) showing the occurrence of plumbogaidonnayite from the Saima lujavrite sample SM 01. (a, b) An aggregate of plumbogaidonnayite as an alteration product in a pseudomorph after eudialyte. (c,d) Plumbogaidonnayite grains (including the holotype crystal selected for Raman spectroscopy and single-crystal XRD determination) associated with other secondary minerals including gaidonnayite, natrolite and britholite-(Ce), and eudialyte relics. Mineral abbreviations after Warr (2021): Ab – albite; Aeg – aegirine; Bri-Ce – britholite-(Ce); Eud – eudialyte; Gdn – gaidonnayite; Mcc – microcline; Ntr – natrolite; Pgdn – plumbogaidonnayite.

silicate minerals (e.g. vigrishinite and zvyaginite, Pekov and Chukanov, 2005; Pekov *et al.*, 2013, 2014). Other hydrothermal Pb-bearing minerals such as galena and gysinite-(La) have also been observed in interstices of microcline in the plumbogaidonnayite-bearing lujavrite samples. The texture and mineral relationships indicate that lead in plumbogaidonnayite was probably derived from external Pb-rich hydrothermal fluids and zirconium from primary eudialyte dissolution ($\text{PbO} < 1 \text{ wt.}\%$, Wu *et al.*, 2016).

Physical and optical properties

Plumbogaidonnayite is transparent, colourless, or light brown in transmitted light with a vitreous lustre. The streak colour is white. It is brittle with a conchoidal fracture, and no cleavage or twinning was observed. The Mohs hardness value is estimated at ~ 5 in analogy with other gaidonnayite-group minerals. The calculated density of plumbogaidonnayite is 3.264 g/cm^3 based on its unit-cell parameters and empirical formula (see below). Optically, it is biaxial (+) with $\alpha = 1.61(3)$, $\beta = 1.63(3)$ and $\gamma = 1.66(4)$ (white light). The calculated $2V$ is 80° , with optical orientation $\alpha \parallel a$, $\beta \parallel b$, and $\gamma \parallel c$. Some physical and optical properties could not be tested owing to the small crystal size. According to its measured refraction indices and calculated density, the compatibility index $[1 - (K_p/K_c)]$ yields 0.053, which belongs to the 'good' category (Mandarino, 1981).

Raman spectroscopy

The Raman spectrum of plumbogaidonnayite was obtained using a Renishaw inVia RM2000 spectrometer at the State Key Laboratory of Nuclear Resources and Environment, East China University of Technology, China. Excitation wavelength and working power were set at 532 nm and 20 mW, respectively. Before collection, a pure silicon standard (520 cm^{-1}) was selected for equipment calibration. In order to get a strong Raman signature and indicate any presence of H_2O , spectrum signals were collected from 100 to 4000 cm^{-1} with a 30 s accumulation time and 2–3 accumulations were adopted.

The Raman characteristics for structural framework in plumbogaidonnayite, which is composed of SiO_4 tetrahedra and ZrO_6 octahedra, are similar to those of gaidonnayite, georgechaoite and isostructural synthetic materials (Celestian *et al.*, 2019, Fig. 2). The strongest Raman band at 521 cm^{-1} is assigned to the symmetric stretching mode of the three-member ring formed by Si1-, Si2- and Zr1-centred polyhedra (see crystal structure below), and the band at 738 cm^{-1} probably represents the mixed vibrations of this ring (Sitarz *et al.*, 2000; Kovalskaya *et al.*, 2023). The second strongest band at 920 cm^{-1} is assigned to the stretching mode of the $[\text{Zr}_1\text{O}_6]$ – $[\text{Si}_2\text{O}_4]$ spiral chain extending along the a axis. The moderate peak at 325 cm^{-1} possibly corresponds to SiO_4 ν_4 antisymmetric bending or lattice vibrations, and 687 cm^{-1} may represent the Si–O–Si bend involving the bridging oxygen. The weak band at 454 cm^{-1} can be assigned to lattice vibrations and other weak bands from 900 to 1100 cm^{-1} (i.e. bands at 1011, 1034 and 1059 cm^{-1}) represent asymmetric Si–O stretching vibrations in SiO_4 tetrahedra, as illustrated in some other species, for example some zeolite-group minerals (Dutta and Del Barco, 1985). The bands of H_2O present at 3486 and 1612 cm^{-1} correspond to the symmetric O–H stretching mode and H–O–H bending mode, respectively (Carey and Korenowski, 1998). In addition, broad bands at 2460 and 3065 cm^{-1} are probably assigned to SiO–H stretching vibrations

or hydrogen bonds in potential hydrated H_3O^+ complexes, which are common in hydrous zirconosilicates (e.g. eudialyte-group minerals, Chukanov *et al.*, 2022; Kovalskaya *et al.*, 2023).

Chemical composition

Chemical composition of plumbogaidonnayite was determined using a JEOL-JXA 8530F Plus electron probe micro-analyser (EPMA) in wavelength dispersive spectroscopy (WDS) mode at 15 kV and 50 nA at the State Key Laboratory of Nuclear Resources and Environment, East China University of Technology, China. A defocused beam (5 μm) was chosen for this hydrous mineral to minimise the element diffusion (e.g. K, Na and Ca). Counting times for stable elements on peaks and background were 20 and 10 s and those for K, Na and Ca were 10 and 5 s, respectively. Standards selected for calibration are listed in Table 1. Calculations on the basis of nine oxygen atoms and assuming the occurrence of two H_2O groups for 23 analyses on different plumbogaidonnayite grains gives the following empirical chemical formula: $(\text{Pb}_{0.70}\text{Ca}_{0.17}\text{Ba}_{0.01}\text{K}_{0.11}\text{Na}_{0.01}\text{Y}_{0.01})_{\Sigma 1.01}(\text{Zr}_{1.00}\text{Hf}_{0.01}\text{Ti}_{0.01})_{\Sigma 1.02}\text{Si}_{3.01}\text{O}_9 \cdot 2\text{H}_2\text{O}$. The ideal formula of $\text{PbZrSi}_3\text{O}_9 \cdot 2\text{H}_2\text{O}$ requires PbO 39.68, ZrO_2 21.89, SiO_2 32.03, $\text{H}_2\text{O}_{\text{calc}}$ 6.40, total 100 (all in wt.%). Some crystals show compositional heterogeneity under back-scattered electron imaging due to variations in K (0.04–0.24 atoms per formula unit), Ca (0.02–0.32 apfu) and Pb (0.62–0.80 apfu, Fig. 1c). Overall, Pb shows a negative relation with K, Na and Ca, implying potential $\text{Pb}^{2+} \rightarrow 2\text{K}^+(\text{Na}^+)$ and $\text{Pb}^{2+} \rightarrow \text{Ca}^{2+}$ substitutions in plumbogaidonnayite (Fig. 3).

Powder X-ray diffraction

The powder X-ray diffraction (XRD) data for plumbogaidonnayite was collected at the School of Earth Sciences and Info-physics, Central South University, China, using a Rigaku XtaLAB Synergy diffractometer ($\text{CuK}\alpha$, $\lambda = 1.54184 \text{ \AA}$) in powder Gandolfi mode. The working voltage and current were set at 50 kV and 1 mA, respectively. The structural model of a single crystal (see below) was used to index the powder XRD pattern of plumbogaidonnayite (Table 2). The nine strongest lines [d in Å (I , %) (hkl)] are: 6.489 (36) (020), 5.803 (100) (101), 4.661 (27) (021), 4.336 (29) (121), 3.640 (30) (221), 3.114 (79) (112), 2.947 (27) (400), 2.622 (27) (241) and 2.493 (27) (312). Refined orthorhombic unit-cell parameters are: $a = 11.7696(5) \text{ \AA}$, $b = 13.0048(4) \text{ \AA}$, $c = 6.6588(4) \text{ \AA}$, $V = 1019.21(5) \text{ \AA}^3$ and $Z = 4$, which were obtained from the powder data using the software program *UnitCell* (Holland and Redfern, 1997).

Crystal structure determination

Single-crystal X-ray diffraction data were collected on the same diffractometer equipped with $\text{CuK}\alpha$ radiation ($\lambda = 1.54184 \text{ \AA}$) at 50 kV and 1 mA. As the sample size is very small (20 μm or less), $\text{CuK}\alpha$ was chosen due to its strong intensity for an X-ray tube of 50 W power giving good quality diffraction data. A relatively homogeneous plumbogaidonnayite crystal ($20 \times 20 \times 20 \mu\text{m}$) was dug from a polished thin section to perform a structure refinement. It contains (in wt.%) SiO_2 34.96–36.36, ZrO_2 23.52–24.90, HfO_2 0.26–0.48, Y_2O_3 0.02–0.55, CaO 1.84–2.74, PbO 28.55–31.63, Na_2O 0.01–0.11 and K_2O 0.43–1.07 based on eight analysis spots in and around the grain, yielding the average

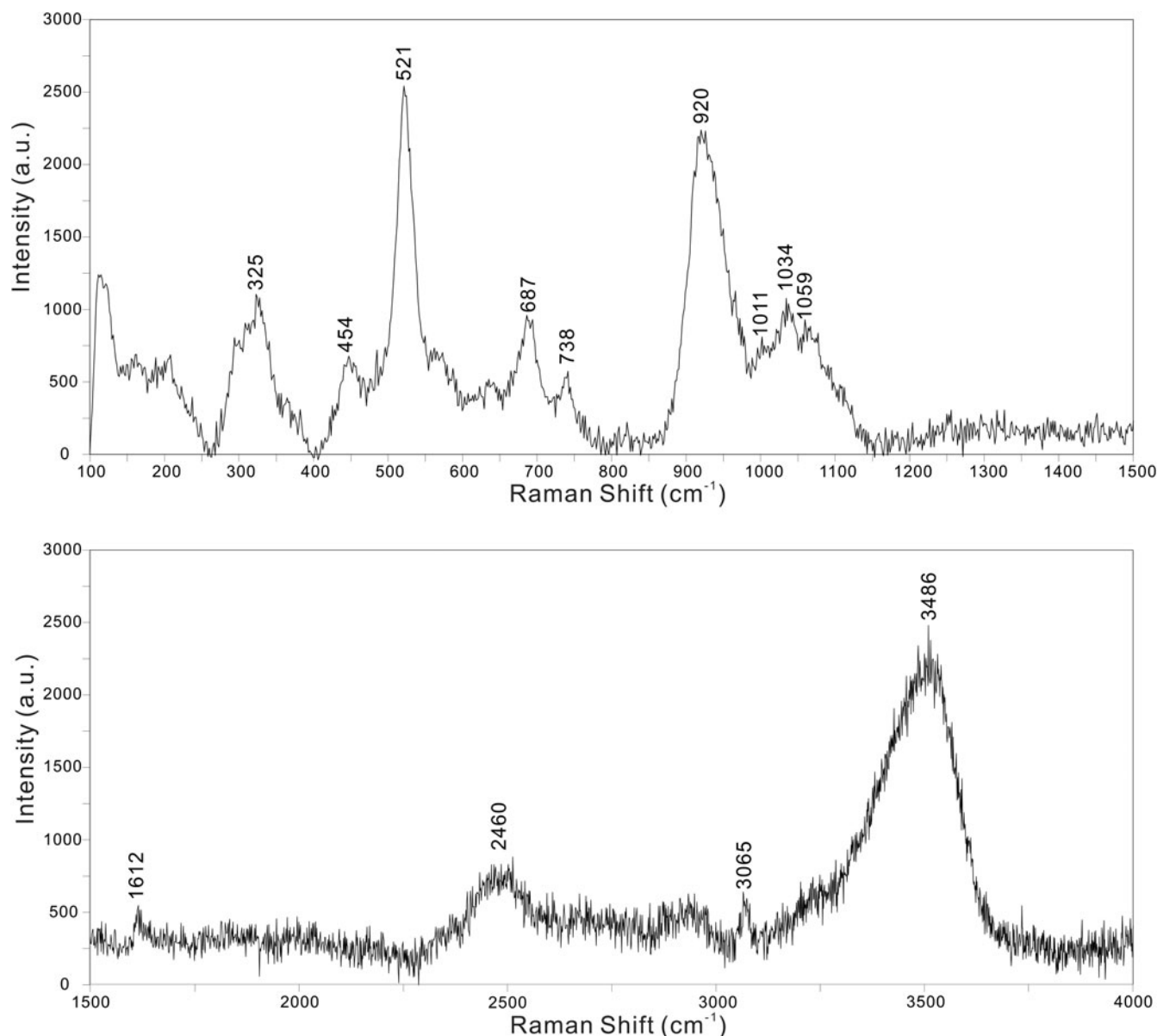


Figure 2. The Raman spectrum for plumbogaidonnayite. a.u. = arbitrary units.

Table 1. Chemical electron microprobe data (in wt.%) for plumbogaidonnayite.

Const.	Mean	Range	S.D. (σ)	Apfu	Standard
SiO ₂	35.34	34.47–36.83	0.57	3.005	Zircon
TiO ₂	0.13	0.02–0.29	0.09	0.008	Rutile
ZrO ₂	24.09	22.79–25.56	0.55	1.000	Zircon
HfO ₂	0.36	0.18–0.62	0.10	0.009	Hf metal
Y ₂ O ₃	0.16	Bdl–0.55	0.15	0.007	Synthetic YPO ₄
CaO	1.86	0.16–3.58	1.22	0.168	Plagioclase
BaO	0.20	0.05–0.35	0.07	0.007	Baryte
PbO	30.52	27.81–34.09	1.55	0.699	Crocoite
Na ₂ O	0.07	Bdl–0.18	0.04	0.012	Jadeite
K ₂ O	1.03	0.35–2.22	0.60	0.113	Orthoclase
H ₂ O*	7.06	6.89–7.36	0.11	2.000	
Total	100.82	100.14–101.53	0.43		

S.D. = standard deviation; Bdl = below detection limits; Apfu = atoms per formula unit; Const. = constituent. *H₂O was assumed as 2 apfu according to the ideal formula of plumbogaidonnayite.

composition $(\text{Pb}_{0.69}\text{Ca}_{0.20}\text{K}_{0.10}\text{Na}_{0.01}\text{Y}_{0.02})_{\Sigma 1.03}(\text{Zr}_{1.00}\text{Hf}_{0.01})_{\Sigma 1.01}\text{Si}_{3.00}\text{O}_9 \cdot 2\text{H}_2\text{O}$. The software *CrysAlis^{Pro}* (Rigaku Oxford Diffraction, UK) and *SHELX* (Sheldrick, 2015a, 2015b) were used for diffraction data processing and structure refinement. The plumbogaidonnayite structure was solved in space group $P2_1nb$ and all sites were first refined with isotropic vibrations. The occupancies of Si, Zr and O were fixed at 1 and those for Pb, Ca, and K were freely refined. The result of $(\text{Pb}_{0.62}\square_{0.38})_{\Sigma 1.00}(\text{Ca}_{0.18}\text{K}_{0.14}\text{Pb}_{0.04}\square_{0.64})_{\Sigma 1.00}\text{ZrSi}_3\text{O}_{11}$ is consistent with the EPMA data. During the refinement, the splitting of Pb into Pb1, Pb2 and Pb3 subsites with low occupancy from the same site was necessary because an unsplit model, similar to those of gaidonnayite and georgechaoite, would lead to unreasonable results with $R_1 = 9.04\%$, shift = 1.044 and a residual maximum = $7.2 \text{ e}^{-\text{\AA}^{-3}}$ around the Pb site (0.990 and 0.898 Å for Pb1–Pb2 and Pb1–Pb3 distances, respectively). In addition, the occupancy of the Pb (Pb1, Pb2 and Pb3) site by Ca and K were also tested but it required too many Ca

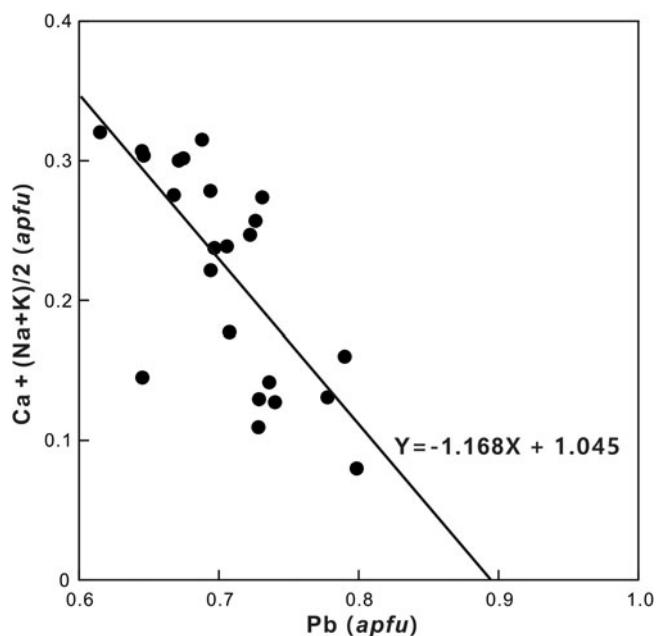


Figure 3. Compositional variations for plumbogaidonnayite plotted on a Pb vs. Ca + (Na+K)/2 diagram. apfu = atoms per formula unit.

(0.62 apfu) and K (0.31 apfu) atoms due to the electron density, which disagreed with the EPMA data. Similarly, the Ca (Ca1, K1 and Pb4) site may also be split due to its unusual displacement parameter ($U_{eq} = 0.311 \text{ \AA}^2$) in an unsplit model, thus, combined with residual electron densities and peaks around the Ca site, we also split it into Ca1, K1 and Pb4 subsites with much lower U_{eq} (0.073, 0.13 and 0.10 \AA^2 , respectively) by isotropic refinement. Anisotropic refinement for these subsites was also tried, but the atoms were nearly overlapped again as in the unsplit model and it led to a non-positive-definite result. The crystal structure refinement finally converged to $R_1 = 5.59\%$ for 1788 unique reflections ($I > 2\sigma(I)$) and 182 parameters. Unit cell parameters refined are: $a = 11.7690(4) \text{ \AA}$, $b = 12.9867(3) \text{ \AA}$, $c = 6.66165(16) \text{ \AA}$, $V = 1018.17(5) \text{ \AA}^3$ and $Z = 4$ in $P2_1nb$. Details for reflections collection and refinement are available in Table 3, and corresponding atom coordinates, site occupancies, equivalent isotropic and

anisotropic atomic displacement parameters are provided in Table 4 and Table 5. Selected bond distances and angles are given in Table 6, and bond-valence sums for each atom are presented in Table 7. The structure of plumbogaidonnayite is shown in Fig. 4. The crystallographic information file has been deposited with the Principal Editor of *Mineralogical Magazine* and is available as Supplementary material (see below).

Plumbogaidonnayite is a new Pb-member of the gaidonnayite-group minerals containing a similar zirconosilicate framework to gaidonnayite and georgechaoite (Chao, 1985; Ghose and Thakur, 1985). It is composed of repeating sinusoidal six $[\text{SiO}_4]$ tetrahedra single-silicate chains extending along $[101]$ and $[10\bar{1}]$ (Fig. 4a), and then chains are corner-linked with $[\text{ZrO}_6]$ octahedra into a three-dimensional framework. However, splitting and disordering occur at the extra-framework sites (including cations and H_2O groups) in the plumbogaidonnayite structure, in the space between the silicate chains and $[\text{ZrO}_6]$ octahedra, which are commonly fully ordered and occupied by Na and K in gaidonnayite and georgechaoite. Of note, the strong disorder in the extra-framework sites would still lead to some physically unreasonable parameters related to these positions, which are assigned based on electron densities and statistical coordinates. For instance, the large U_{eq} values (0.126(13) and 0.146(15) \AA^2) for H_2O groups may suggest partial occupancy at the O10 and O11 sites. In addition, some short distances between extra-framework sites, such as Pb2–O10 (2.09(3) \AA), K1–O11 (1.47(14) \AA), Pb1–Ca1 (2.24(5) \AA), Pb2–Ca1 (2.33(5) \AA), Pb3–Pb4 (2.29(9) \AA) and Pb3–K1 (3.18(15) \AA), could indicate the mutually exclusive occupancy of these two positions or potentially partial H_2O groups involved at these disordered cation sites.

Si–O tetrahedra

In plumbogaidonnayite, three crystallographically distinct Si1, Si2 and Si3 sites in SiO_4 tetrahedra are fully occupied by Si with average Si–O bond distances of 1.628 (Si1–O), 1.615 (Si2–O) and 1.614 (Si3–O) \AA . These tetrahedra form a basic repeating sinusoidal six $[\text{SiO}_4]$ tetrahedra single $[\text{Si}_6\text{O}_{18}]^{12-}$ chain by corner-sharing (Fig. 4a). The Si–O–Si angles which involve bridging oxygen range from 133.0 to 135.2° with an average of 134.4°. The average bridging Si–O distance (1.629 \AA) is longer than that

Table 2. Measured and calculated* powder X-ray diffraction data (d in \AA , I in %) for plumbogaidonnayite.

l_{meas}	l_{calc}	d_{meas}	d_{calc}	$h k l$	l_{meas}	l_{calc}	d_{meas}	d_{calc}	$h k l$	l_{meas}	l_{calc}	d_{meas}	d_{calc}	$h k l$
36	100	6.489	6.493	0 2 0	1	4	2.569	2.576	1 3 2	6	2	1.761	1.765	3 3 3
100	42	5.803	5.797	1 0 1	27	17	2.493	2.492	3 1 2	9	5	1.748	1.744	4 6 0
9	7	5.309	5.294	1 1 1	1	2	2.415	2.409	2 3 2	2	2	1.710	1.710	2 7 1
27	40	4.661	4.650	0 2 1	3	3	2.367	2.370	1 5 1	8	2	1.684	1.687	5 5 1
29	34	4.336	4.326	1 2 1	3	2	2.284	2.281	1 4 2	8	4	1.627	1.628	6 4 1
24	17	4.181	4.176	2 1 1	8	7	2.217	2.219	5 0 1	1	3	1.609	1.606	1 7 2
30	29	3.640	3.648	2 2 1	7	14	2.167	2.164	0 6 0	5	3	1.569	1.563	1 8 1
21	24	3.469	3.469	1 3 1	4	5	2.103	2.100	5 2 1	1	1	1.550	1.550	5 6 1
17	15	3.361	3.358	3 2 0	14	12	2.052	2.051	2 1 3	2	1	1.513	1.513	5 3 3
9	2	3.242	3.271	3 1 1	4	3	2.030	2.028	1 6 1	7	3	1.494	1.498	3 7 2
79	47	3.114	3.111	1 1 2	12	6	1.967	1.965	4 3 2	3	1	1.462	1.461	6 1 3
27	28	2.947	2.942	4 0 0	6	5	1.946	1.943	2 6 1	7	2	1.419	1.421	4 8 0
11	2	2.825	2.829	2 1 2	2	2	1.904	1.896	3 6 0	4	3	1.386	1.384	2 7 3
15	11	2.659	2.664	3 3 1	3	4	1.863	1.862	6 1 1	3	2	1.372	1.372	5 5 3
27	24	2.622	2.615	2 4 1	4	3	1.810	1.807	6 2 1					

*The calculated values were obtained using VESTA 3 (Momma and Izumi, 2011). The strongest values are given in bold.

Table 3. Data collection and structure refinement details for plumbogaidonnayite.

Crystal data	
Ideal formula	PbZrSi ₃ O ₉ ·2H ₂ O
Crystal dimensions (mm)	0.020 × 0.020 × 0.020
Crystal system, space group	Orthorhombic, <i>P2₁nb</i>
Temperature (K)	293(2)
<i>a</i> (Å)	11.7690(4)
<i>b</i> (Å)	12.9867(3)
<i>c</i> (Å)	6.66165(16)
<i>V</i> (Å ³)	1018.17(5)
<i>Z</i>	4
Calculated density (g·cm ⁻³)	3.264
Data collection	
Crystal description	Colourless platy crystal
Working voltage (kV) and current (mA)	50, 1
Instrument	Rigaku XtaLAB Synergy
Radiation type, wavelength (Å)	CuKα, 1.54184
Absorption coefficient, μ (mm ⁻¹)	34.716
<i>F</i> (000)	921
θ range (°)	6.818 to 77.55
No. of measured, independent and observed [<i>I</i> > 2σ(<i>I</i>)] reflections	5989, 1859, 1788
<i>R</i> _{int}	0.0554
Indices range of <i>h</i> , <i>k</i> , <i>l</i>	-14 ≤ <i>h</i> ≤ 14, -16 ≤ <i>k</i> ≤ 12, -8 ≤ <i>l</i> ≤ 8
Refinement	
Refinement	Full-matrix least squares on <i>F</i> ²
Number of reflections, restraints, parameters	1859, 1, 182
<i>R</i> ₁ [<i>I</i> > 2σ(<i>I</i>)], <i>R</i> ₁ (all)	0.0559, 0.0576
<i>wR</i> ₂ [<i>I</i> > 2σ(<i>I</i>)], <i>wR</i> ₂ (all)*	0.1345, 0.1355
GoF	1.114
Δρ _{max} , Δρ _{min} (e Å ⁻³)	1.29, -1.17
Flack parameter [#]	0.072(12)

**wR*₂ = {Σ[w(*F*_o² - *F*_c²)²]/Σ[w(*F*_o²)]^{1/2}}; *w* = 1/[σ(*F*_o)² + (*aP*)² + *bP*] where *a* is 0.0454, *b* is 17.9195 and *P* is [2*F*_o² + Max(*F*_o, 0)]/3.

[#]Flack parameter is calculated from Flack (1983).

of non-bridging Si–O bonds (1.608 Å), and the average O–Si–O angle involving the bridging bonds (106.5°) is smaller than that with the non-bridging bonds (113.1°). These so-called ‘²*T*₆ chains’ and similar trends of the Si–O bond and O–Si–O angle also exist in gaidonnayite, georgechaoite, stokesite and some

synthetic materials (Day and Hawthorne, 2020 and references therein). The calculated bond-valence sum (BVS) for Si1 (4.04 valence units), Si2 (4.20 vu) and Si3 (4.21 vu) are close to the ideal values within error (Table 7).

Zr–O octahedra

The Zr–O bond distances in relatively regular octahedra range from 2.056 to 2.154 Å with an average length of 2.094 Å. A single ZrO₆ octahedron is corner-linked with three different [Si₆O₁₈]¹²⁻ chains by sharing two oxygen atoms within each chain. These ZrO₆ octahedra and SiO₄ tetrahedra form 7-member rings and 3-member rings from the view nearly along the *c* axis (Fig. 4b), as is also present in other gaidonnayite-group minerals. The ZrO₆ octahedron in plumbogaidonnayite tends to link with disordered Pb (Pb1, Pb2 and Pb3) atoms via face- and edge-sharing, and with Ca (Ca1, K1 and Pb4) atoms via corner-sharing, whereas in the gaidonnayite and georgechaoite structure it shares O–O edges with Na(K)–O octahedra (Chao, 1985; Ghose and Thakur, 1985).

Pb–O polyhedra

The Pb in plumbogaidonnayite tends to occupy the Na2 site of the two Na sites in gaidonnayite, and it splits into three disordered sites, Pb1, Pb2 and Pb3 with occupancies of 0.461(9), 0.099(7) and 0.057(9), respectively (Fig. 4c). Distances for Pb1–Pb2, Pb1–Pb3 and Pb2–Pb3 are 0.935(16), 0.88(5) and 1.23(5) Å, respectively. Pb1 is coordinated to three oxygen atoms (O1, O7 and O8) and two H₂O groups (O10 and O11), with three moderate Pb1–O bond lengths ranging from 2.396(14) to 2.661(14) Å and two Pb1–H₂O lengths of 2.30(4) and 2.67(3) Å, respectively. In contrast, Na–H₂O bonds are normally shorter than other Na–O bonds in Na–O octahedra in gaidonnayite and georgechaoite. The Pb1–O polyhedron shares a face (O1–O7–O8) with an adjacent ZrO₆ octahedron and a corner (O1) with an adjacent SiO₄ tetrahedron. Pb2 is coordinated to four oxygen atoms (O1, O5, O7 and O9), and the Pb2–O polyhedron shares two edges (O5–O9 and O5–O7) with ZrO₆

Table 4. Wyckoff positions, atom coordinates, inferred site occupancies, and equivalent isotropic displacement parameters in the plumbogaidonnayite structure.

Atom	Occupancy	Wyckoff	<i>x</i>	<i>y</i>	<i>z</i>	<i>U</i> _(eq)
Pb1	Pb _{0.461(9)}	4 <i>a</i>	0.9642(2)	0.06272(19)	0.6546(4)	0.0352(11)
Pb2	Pb _{0.099(7)}	4 <i>a</i>	0.0071(10)	0.0776(6)	0.769(3)	0.045(5)
Pb3	Pb _{0.057(9)}	4 <i>a</i>	0.025(4)	0.029(3)	0.614(6)	0.101(17)
Ca1	Ca _{0.18(4)}	4 <i>a</i>	0.593(4)	0.063(3)	0.390(7)	0.073(18)
K1	K _{0.14(5)}	4 <i>a</i>	0.722(12)	0.138(9)	0.404(14)	0.13(5)
Pb4	Pb _{0.040(11)}	4 <i>a</i>	0.649(6)	0.107(5)	0.393(7)	0.10(2)
Zr1	Zr	4 <i>a</i>	0.24999(13)	0.06308(10)	0.13398(18)	0.0206(5)
Si1	Si	4 <i>a</i>	0.7279(4)	0.2051(4)	0.8832(6)	0.0253(11)
Si2	Si	4 <i>a</i>	0.5098(5)	0.0842(3)	0.8943(6)	0.0212(9)
Si3	Si	4 <i>a</i>	0.3026(4)	0.1173(3)	0.6379(6)	0.0197(9)
O1	O	4 <i>a</i>	0.2968(12)	-0.0970(9)	0.1520(17)	0.026(3)
O2	O	4 <i>a</i>	0.5944(12)	0.1808(10)	0.932(2)	0.034(3)
O3	O	4 <i>a</i>	0.7775(12)	0.2618(9)	0.0825(16)	0.029(3)
O4	O	4 <i>a</i>	0.7321(11)	0.2820(8)	0.6932(17)	0.025(3)
O5	O	4 <i>a</i>	0.5797(11)	-0.0196(9)	0.8603(19)	0.029(3)
O6	O	4 <i>a</i>	0.4367(11)	0.1096(10)	0.6922(17)	0.030(3)
O7	O	4 <i>a</i>	0.4250(11)	0.0725(10)	0.0827(19)	0.029(3)
O8	O	4 <i>a</i>	0.2829(13)	0.0485(9)	0.4453(17)	0.031(3)
O9	O	4 <i>a</i>	0.2282(11)	0.0848(10)	0.8307(14)	0.024(3)
O10 (H ₂ O)	O	4 <i>a</i>	0.018(3)	0.231(2)	0.866(5)	0.126(13)
O11 (H ₂ O)	O	4 <i>a</i>	0.844(4)	0.1524(19)	0.448(5)	0.146(14)

Table 5. Anisotropic displacement parameters (in Å²) for plumbogaidonnayite.

Atom	U^{11}	U^{22}	U^{33}	U^{23}	U^{13}	U^{12}
Pb1	0.0340(17)	0.0379(13)	0.0337(15)	0.0074(8)	0.0071(11)	-0.0045(10)
Pb2	0.034(6)	0.036(5)	0.065(11)	0.000(4)	0.010(7)	-0.004(4)
Pb3	0.08(3)	0.13(3)	0.09(2)	0.04(2)	0.01(2)	0.03(2)
Zr1	0.0242(8)	0.0240(7)	0.0135(6)	-0.0026(5)	0.0019(6)	-0.0057(6)
Si1	0.027(3)	0.029(2)	0.0196(19)	-0.0018(16)	-0.0002(19)	-0.0036(18)
Si2	0.020(2)	0.026(2)	0.0176(19)	-0.0017(16)	-0.0002(18)	-0.0004(18)
Si3	0.026(2)	0.0237(19)	0.0096(16)	-0.0010(15)	0.0006(17)	0.0022(17)
O1	0.033(6)	0.022(5)	0.023(5)	0.005(4)	-0.003(5)	0.007(5)
O2	0.031(7)	0.034(6)	0.036(7)	-0.005(5)	-0.006(6)	-0.006(5)
O3	0.045(9)	0.023(5)	0.018(5)	0.009(4)	-0.002(5)	-0.005(5)
O4	0.033(7)	0.015(5)	0.027(5)	0.000(4)	0.005(5)	0.001(5)
O5	0.027(6)	0.028(6)	0.031(7)	-0.007(5)	-0.002(5)	0.010(5)
O6	0.032(7)	0.043(7)	0.016(5)	-0.001(5)	0.010(5)	0.002(6)
O7	0.026(7)	0.040(7)	0.023(6)	0.001(5)	0.005(6)	0.001(5)
O8	0.049(8)	0.034(6)	0.010(5)	0.002(4)	0.003(5)	-0.008(6)
O9	0.028(7)	0.042(7)	0.003(4)	-0.003(4)	0.003(5)	-0.011(5)
O10 (H ₂ O)	0.077(19)	0.096(18)	0.21(4)	-0.017(19)	0.04(2)	0.016(16)
O11 (H ₂ O)	0.23(4)	0.056(14)	0.15(3)	-0.060(16)	-0.03(3)	0.017(19)

octahedron and Si₂O₄ tetrahedron, and two corners (O1 and O9) with SiO₄ and Si₃O₄ tetrahedra, respectively. The short Pb2–O10 distance of 2.09(3) Å may be a result of the statistically average positions of the extra-framework atoms, or indicates the mutually exclusive occupancy of these two positions. Pb3 is coordinated to three oxygen atoms (O6, O7 and O9) and one H₂O molecule (O11) with an average length of 2.84 Å. The Pb3–O polyhedron shares oxygen (O6, O7 and O9) corners with adjacent ZrO₆ octahedron and SiO₄ (Si2 and Si3) tetrahedra.

Ca–O polyhedra

The Ca in plumbogaidonnayite tends to occupy the Na1 site of the two Na sites in gaidonnayite, which splits into different Ca1, K1 and Pb4 subsites with occupancies of 0.18(4), 0.14(5) and 0.040(11), respectively (Fig. 4c). Distances for Ca1–K1, Ca1–Pb4 and K1–Pb4 bonds are 1.81(15), 0.87(7) and 0.95(16) Å, respectively. Ca1 is bound to one oxygen atom (O6) and one H₂O group (O10) with distances of 2.79(5) Å and 2.83(5) Å. Four K1–O (O1, O3, O4 and O8) bonds range from 2.69(11) to 3.13(10) Å. The K1–O polyhedron is corner-linked with SiO₄,

Table 6. Selected bond distances (Å) and angles (°) for plumbogaidonnayite.

Si–O tetrahedra				Bond angles in Si–O tetrahedra			
Si1–O1	1.638(14)	Si2–O2	1.621(13)	Si3–O3	1.640(12)	O–Si1–O ^{mean}	109.4
Si1–O2	1.636(15)	Si2–O5	1.595(12)	Si3–O6	1.622(14)	O–Si2–O ^{mean}	109.5
Si1–O3	1.626(12)	Si2–O6	1.631(13)	Si3–O8	1.581(13)	O–Si3–O ^{mean}	109.4
Si1–O4	1.613(12)	Si2–O7	1.611(14)	Si3–O9	1.611(11)		
<Si1–O>	1.628	<Si2–O>	1.615	<Si3–O>	1.614		
Pb–O polyhedra				Ca–O polyhedra			
Pb1–O1	2.396(14)	Pb3–O6	2.91(5)	Ca1–O6	2.79(5)	Bond angles between Si–O tetrahedra	
Pb1–O7	2.522(13)	Pb3–O7	2.68(4)	Ca1–O10	2.83(5)	Si1–O2–Si2	135.1(9)
Pb1–O8	2.661(14)	Pb3–O9	2.89(5)	<Ca1–O>	2.81	Si1–O2–Si3	133.0(7)
Pb1–O10	2.67(3)	Pb3–O11	2.89(6)			Si2–O6–Si3	135.2(8)
Pb1–O11	2.30(4)	<Pb3–O>	2.84	K1–O1	3.13(10)		
<Pb1–O>	2.510			K1–O3	2.76(10)		
				K1–O4	2.69(11)		
Pb2–O1	2.542(18)			K1–O8	2.72(10)		
Pb2–O5	2.72(2)			K1–O10	2.96(12)		
Pb2–O7	2.388(16)			<K1–O>	2.85		
Pb2–O9	2.637(18)						
Pb2–O10	2.09(3)			Pb4–O8	2.78(7)		
<Pb2–O>	2.475			Pb4–O10	2.62(6)		
				Pb4–O11	2.40(9)		
				<Pb4–O>	2.60		
Zr–O octahedra				Cation distances			
Zr1–O1	2.154(11)			Pb1–Pb2	0.935(16)		
Zr1–O4	2.061(10)			Pb1–Pb3	0.88(5)		
Zr1–O5	2.082(13)			Pb2–Pb3	1.23(5)		
Zr1–O7	2.092(13)			Ca1–K1	1.81(15)		
Zr1–O8	2.118(11)			Ca1–Pb4	0.87(7)		
Zr1–O9	2.056(9)			K1–Pb4	0.95(16)		
<Zr1–O>	2.094						

Table 7. Calculated bond valence sums (in vu) of atoms for plumbogaidonnayite.*

	Zr1	Si1	Si2	Si3	Pb ^a	Ca ^b	Total
O1	0.56	0.98			0.32		1.86
O2		0.99	1.03				2.02
O3		1.02		0.98			2.00
O4	0.72	1.05					1.77
O5	0.68		1.11		0.03		1.82
O6			1.00	1.03		0.02	2.05
O7	0.66		1.06		0.27	0.02	2.01
O8	0.61			1.14	0.14	0.05	1.94
O9	0.73			1.06	0.03	0.03	1.85
O10 (H ₂ O)					0.27	0.06	0.33
O11 (H ₂ O)					0.37	0.07	0.44
Total	3.96	4.04	4.20	4.21	1.43	0.25	

*Bond-valence sums were calculated with the site occupancy given in Table 4, using the parameters of Brese and O'Keeffe (1991).

^a(Pb1, Pb2, Pb3); ^b(Ca1, K1, Pb4)

SiO₄ tetrahedra and a ZrO₆ octahedron, and also shares an O3–O4 edge with a SiO₄ tetrahedron and an O1–O8 edge with a ZrO₆ octahedron, respectively. The short K1–O11 distance (1.47(14) Å) may indicate that these two atoms cannot be occupied simultaneously, or the possibility of H₂O groups at these disordered extra-framework cations. The Pb4–O polyhedron is corner-linked (O8) with a SiO₄ tetrahedron and a ZrO₆ octahedron. The Pb4–O8 bond distance (2.78(7) Å) is longer than Pb4–H₂O (O10 and O11) bonds (2.62(6) Å and 2.40(9) Å, respectively).

Implications

Plumbogaidonnayite is the first naturally discovered divalent cation-dominant member of the gaidonnayite-group minerals, which occurs associated closely with hydrothermal gaidonnayite and georgechaoite after eudialyte alteration. In actuality, the latter two are common alteration products after eudialyte in peralkaline complexes and eudialyte dissolution experiments (Ivanyuk *et al.*, 2015; Borst *et al.*, 2016; Mikhailova *et al.*, 2022), however the absence of plumbogaidonnayite in most cases is probably attributed to a lack of Pb-rich metasomatic fluids. In contrast, late Sr–Pb-rich fluid activity was pervasive in the Saima alkaline complex (Wu *et al.*, 2015, 2018), which resulted in the replacement of primary zirconosilicates (e.g. wadeite and eudialyte) by a variety of hydrothermal minerals including plumbogaidonnayite, calcite and strontianite, as well as the formation of the newly approved fluorsigaiite and gysinite-(La) (Wu *et al.*, 2022, 2023a).

Ion exchange occurs widely in gaidonnayite-group minerals and similar zirconosilicates (e.g. catapleiteite- and hilairite-group minerals) under natural and experimental conditions (Pushcharovskii *et al.*, 2002; Aksenov *et al.*, 2016; Celestian *et al.*, 2019). Recent experimental work has demonstrated that Cs⁺ could exchange at the extra-framework cation (Na) site into the gaidonnayite structure from room temperature to 95°C (Celestian *et al.*, 2019), which implies that plumbogaidonnayite could crystallise from eudialyte alteration or its alteration product (e.g. gaidonnayite and georgechaoite) in a naturally low-temperature fluid environment. In comparison with isovalent substitution, heterovalent ion exchange in isomorphism would

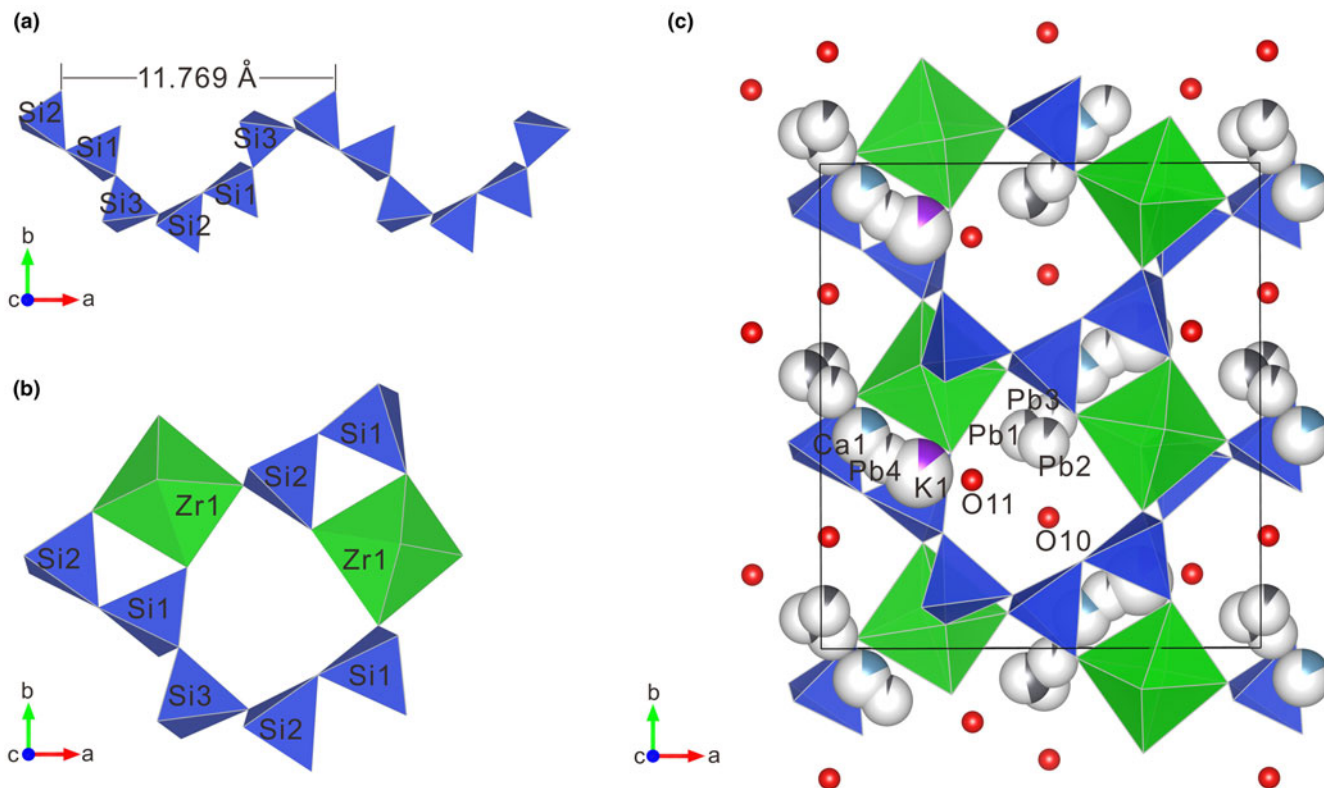


Figure 4. Crystal structure of plumbogaidonnayite (unit cell outlined in black lines) plotted with VESTA 3 (Momma and Izumi, 2011). (a) The repeating sinusoidal six [SiO₄] tetrahedra single-silicate chain. (b) ZrO₆ octahedra and SiO₄ tetrahedra forming a 7-member ring and 3-member ring from the view along the c axis. (c) Disordered Pb (Pb1, Pb2 and Pb3), Ca (Ca1, K1 and Pb4) and two H₂O groups (O10 and O11) distributed over the space between the ZrO₆-SiO₄ framework (modified after Wu *et al.*, 2023c).

not only influence the main Raman vibrational features and unit-cell parameters, but also tends to cause more vacancies at the extra-framework cation sites and decrease the symmetry, as demonstrated by $\text{Na}^+ \rightarrow \text{Ca}^{2+}$ exchanges in calciccatapleite and calciophilairite, $\text{Na}^+ \rightarrow \text{Zn}^{2+}$ exchanges in vigrishinite and zvyaginite, and $\text{Na}^+ \rightarrow \text{Pb}^{2+}$ exchange in plumbogaidonnayite (Pushcharovskii *et al.*, 2002; Pekov *et al.*, 2013, 2014; Aksenov *et al.*, 2016). However, although Ca occupies the NaI site over other cations (except vacancies) during our plumbogaidonnayite structure refinement, the Ca member of gaidonnayite has never been discovered in natural samples, probably due to compositional similarity to calciccatapleite (Mandarino and Sturman, 1978; Ilyushin *et al.*, 1981). Nevertheless, the discovery of plumbogaidonnayite draws attention to the heterovalent substitution and structural disordering in gaidonnayite-group minerals.

Acknowledgements. Professor Igor V. Pekov and two anonymous reviewers are sincerely appreciated for their constructive comments. Dr. Kai Qu is thanked for his generous help in crystal refinement. This study was financially supported by the National Natural Science Foundation of China (Grant No. 42272087 and 42072054), and the Natural Science Foundation of Jiangxi Province, China (Grant No. 20224ACB213012, 20212BAB203003 and 20232BCJ23003).

Supplementary material. The supplementary material for this article can be found at <https://doi.org/10.1180/mgm.2024.2>.

Competing interests. The authors declare none.

References

- Aksenov S.M., Portnov A.M., Chukanov N.V., Rastsvetaeva R.K., Nelyubina Y.N., Kononkova N.N. and Akimenko M.I. (2016) Ordering of calcium and vacancies in calcium catapleite $\text{CaZr}[\text{Si}_3\text{O}_9] \cdot 2\text{H}_2\text{O}$. *Crystallography Reports*, **61**, 376–382.
- Boggs R.C. and Ghose S. (1985) Georgechaoite $\text{NaKZrSi}_3\text{O}_9 \cdot 2\text{H}_2\text{O}$, a new mineral species from Wind Mountain, New Mexico. *The Canadian Mineralogist*, **23**, 1–4.
- Borst A.M., Friis H., Andersen T., Nielsen T.F.D., Waight T.E. and Smit M.A. (2016) Zirconosilicates in the kakortokites of the Ilimaussaq complex, South Greenland: Implications for fluid evolution and high-field-strength and rare-earth element mineralization in apatitic systems. *Mineralogical Magazine*, **80**, 5–30.
- Brese N.E. and O’Keeffe M. (1991) Bond-valence parameters for solids. *Acta Crystallographica*, **B47**, 192–197.
- Carey D.M. and Korenowski G.M. (1998) Measurement of the Raman spectrum of liquid water. *Journal of Chemical Physics*, **108**, 2669–2675.
- Celestian A.J., Lively J. and Xu W.Q. (2019) In situ Cs and H exchange into gaidonnayite and proposed mechanisms of ion diffusion. *Inorganic Chemistry*, **58**, 1911–1928.
- Chao G.Y. (1985) The crystal structure of gaidonnayite $\text{Na}_2\text{ZrSi}_3\text{O}_9 \cdot 2\text{H}_2\text{O}$. *The Canadian Mineralogist*, **23**, 11–15.
- Chao G.Y. and Watkinson D.H. (1974) Gaidonnayite, $\text{Na}_2\text{ZrSi}_3\text{O}_9 \cdot 2\text{H}_2\text{O}$, a new mineral from Mont St. Hilaire, Quebec. *The Canadian Mineralogist*, **12**, 316–319.
- Chukanov N.V., Vigasina M.F., Rastsvetaeva R.K., Aksenov S.M., Mikhailova J.A. and Pekov I.V. (2022) The evidence of hydrated proton in eudialyte-group minerals based on Raman spectroscopy data. *Journal of Raman Spectroscopy*, **53**, 1188–1203.
- Day M.C. and Hawthorne F.C. (2020) A structure hierarchy for silicate minerals: chain, ribbon, and tube silicates. *Mineralogical Magazine*, **84**, 165–244.
- Dutta P.K. and Del Barco B. (1985) Raman spectroscopic studies of zeolite framework. Hydrated zeolite and the influence of cations. *The Journal of Physical Chemistry*, **89**, 1861–1865.
- Flack H.D. (1983) On enantiomorph-polarity estimation. *Acta Crystallographica*, **A39**, 876–881.
- Ghose S. and Thakur P. (1985) The crystal structure of georgechaoite $\text{NaKZrSi}_3\text{O}_9 \cdot 2\text{H}_2\text{O}$. *The Canadian Mineralogist*, **23**, 5–10.
- Hatert F. and Burke E.A.J. (2008) The IMA-CNMNC dominant-constituent rule revisited and extended. *The Canadian Mineralogist*, **46**, 717–728.
- Holland T.J.B. and Redfern S.A.T. (1997) Unit cell refinement from powder diffraction data: the use of regression diagnostics. *Mineralogical Magazine*, **61**, 65–77.
- Ilyushin G.D., Voronkov A.A., Ilyukhin V.V., Nevskii N.N. and Belov N.V. (1981) Crystal structure of natural monoclinic catapleite, $\text{Na}_2\text{ZrSi}_3\text{O}_9 \cdot 2\text{H}_2\text{O}$. *Doklady Akademii Nauk SSSR*, **260**, 623–627.
- Ivanyuk G.Y., Pakhomovsky Y.A. and Yakovenchuk V.N. (2015) Eudialyte-group minerals in rocks of Lovozero layered complex at Mt. Karnasurt and Mt. Kedykvyrpakhk. *Geology of Ore Deposits*, **57**, 600–613.
- Kovalskaya T.N., Ermolaeva V.N., Chukanov N.V., Varlamov D.A., Kovalskiy G.A., Zakharchenko E.S., Kalinin G.M. and Chaichuk K.D. (2023) Synthesis of Fe-deficient eudialyte analogues: Relationships between the composition of the reaction system and crystal-chemical features of the products. *Mineralogical Magazine*, **87**, 233–240.
- Kuznicki S.M., Bell V.A., Nair S., Hillhouse H.W., Jacobinas R.M., Braunbarth C.M., Toby B.H. and Tsapatsis M.A. (2001) Titanosilicate molecular sieve with adjustable pores for size-selective adsorption of molecules. *Nature*, **412**, 720–724.
- Ma D.Z. and Liu Y. (2023) Nb mineralization in the nepheline syenite in the Saima area of the North China Craton, China. *Ore Geology Reviews*, **152**, 105247.
- Mandarino J.A. (1981) The Gladstone-Dale relationship: part IV. The compatibility concept and its application. *The Canadian Mineralogist*, **19**, 441–450.
- Mandarino J.A. and Sturman B.D. (1978) The identity of α -catapleite and gaidonnayite. *The Canadian Mineralogist*, **16**, 195–198.
- Mikhailova J.A., Pakhomovsky Y.A., Kalashnikova G.O. and Aksenov S.M. (2022) Dissolution of the eudialyte-group minerals: experimental modeling of natural processes. *Minerals*, **12**, 1460.
- Momma K. and Izumi F. (2011) VESTA 3 for three-dimensional visualization of crystal, volumetric and morphology data. *Journal of Applied Crystallography*, **44**, 1272–1276.
- Mumpton F. A. (1999) La roca magica: uses of natural zeolites in agriculture and industry. *Proceedings of the National Academy of Science*, **96**, 3463–3470.
- Pekov I.V. and Chukanov N.V. (2005) Microporous framework silicate minerals with rare and transition elements: minerogenetic aspects. Pp. 145–171 in: *Micro- and Mesoporous Mineral Phases* (Giovanni Ferraris and Stefano Merlino, editors). Reviews in Mineralogy & Geochemistry, **57**. Mineralogical Society of America and the Geochemical Society, Chantilly, Virginia, USA.
- Pekov I.V., Britvin S.N., Zubkova N.V., Chukanov N.V., Bryzgalov I.A., Lykova I.S., Belakovskiy D.I. and Pushcharovskiy D.Y. (2013) Vigrishinite, $\text{Zn}_2\text{Ti}_4\text{Si}_4\text{O}_{14}(\text{OH},\text{H}_2\text{O})_8$, a new mineral from the Lovozero alkaline complex, Kola Peninsula, Russia. *Geology of Ore Deposits*, **55**, 575–586.
- Pekov I.V., Lykova I.S., Chukanov N.V., Yapaskurt V.O., Belakovskiy D.I., Zolotarev A.A., Jr. and Zubkova N.V. (2014) Zvyaginite $\text{NaZnNb}_2\text{Ti}[\text{Si}_2\text{O}_7]_2\text{O}(\text{OH},\text{F})_3(\text{H}_2\text{O})_{4+x}$ ($x < 1$), a new mineral of the epistolite group from the Lovozero alkaline pluton, Kola peninsula, Russia. *Geology of Ore Deposits*, **56**, 644–656.
- Pushcharovskii D.Y., Pekov I.V., Pasero M., Gobechiya E.R., Merlino S. and Zubkova N.V. (2002) Crystal structure of cation-deficient calciophilairite and possible mechanisms of decationization in mixed-framework minerals. *Crystallography Reports*, **47**, 748–752.
- Sheldrick G.M. (2015a) SHELXT – Integrated space-group and crystal structure determination. *Acta Crystallographica*, **A71**, 3–8.
- Sheldrick G.M. (2015b) Crystal structure refinement with SHELX. *Acta Crystallographica*, **C71**, 3–8.
- Shen G.F., Xu J.S., Yao P. and Li G.W. (2017) Fengchengite: a new species with the Na-poor but vacancy-dominant N(5) site in the eudialyte group. *Acta Mineralogica Sinica*, **37**, 140–151 [in Chinese with English abstract].
- Sitarz M., Handke M. and Mozgawa W. (2000) Identification of silicoxygen rings in SiO_2 based on IR spectra. *Spectrochimica Acta*, **A56**, 1819–1823.
- Warr L.N. (2021) IMA-CNMNC approved mineral symbols. *Mineralogical Magazine*, **85**, 291–320.

- Wu F.Y., Yang Y.H., Marks M.A.W., Liu Z.C., Zhou Q., Ge W.C., Yang J.S., Zhao Z.F., Mitchell R.H. and Markl G. (2010) In situ U–Pb, Sr, Nd and Hf isotopic analysis of eudialyte by LA-(MC)-ICP-MS. *Chemical Geology*, **273**, 8–34.
- Wu B., Wang R.C., Yang J.H., Wu F.Y., Zhang W.L., Gu X.P. and Zhang A.C. (2015) Wadeite ($K_2ZrSi_3O_9$), an alkali-zirconosilicate from the Saima agpaite rocks in northeastern China: its origin and response to multi-stage activities of alkaline fluids. *Lithos*, **224–225**, 126–142.
- Wu B., Wang R.C., Yang J.H., Wu F.Y., Zhang W.L., Gu X.P. and Zhang A.C. (2016) Zr and REE mineralization in sodic lujavrite from the Saima alkaline complex, northeastern China: A mineralogical study and comparison with potassic rocks. *Lithos*, **262**, 232–246.
- Wu B., Wang R.C., Liu X.D., Guo G.L. and Song Z.T. (2018) Chemical composition and alteration assemblages of eudialyte in the Saima alkaline complex, Liaoning Province, and its implication for alkaline magmatic–hydrothermal evolution. *Acta Petrologica Sinica*, **6**, 1741–1757 [in Chinese with English abstract].
- Wu B., Gu X.P., Rao C., Wang R.C., Xing X.Q., Zhong F.J., Wan J.J. and Bonnetti C. (2022) Fluorsigaiite, $Ca_2Sr_3(PO_4)_3F$, a new mineral of the apatite supergroup from the Saima alkaline complex, Liaoning Province, China. *Mineralogical Magazine*, **86**, 940–947.
- Wu B., Gu X.P., Rao C., Wang R.C., Xing X.Q., Wan J.J., Zhong F.J. and Bonnetti C. (2023a) Gysinite-(La), $PbLa(CO_3)_2(OH)\cdot H_2O$, a new rare earth mineral of the ancylite group from the Saima alkaline complex, Liaoning Province, China. *Mineralogical Magazine*, **87**, 143–150.
- Wu B., Gu X.P., Rao C., Wang R.C., Xing X.Q., Wan J.J. and Zhong F.J. (2023b) Plumbogaidonnayite, IMA 2022-095. CNMNC Newsletter 71, *European Journal of Mineralogy*, **35**, 75–79.
- Wu B., Gu X.P., Wang R.C., Liu X.C., Xing X.Q., and Ren Q. (2023c) Discovery and genesis of three critical metal-bearing minerals. *Geological Review*, **69**, <https://doi.org/10.16509/j.georeview.2023.s1.083> [in Chinese].
- Yang Z.M., Giester G., Ding K.S. and Tillmanns E. (2012) Hezuolinite, $(Sr, REE)_4Zr(Ti, Fe^{3+}, Fe^{2+})_2Ti_2O_8(Si_2O_7)_2$, a new mineral species of the chevkinite group from Saima alkaline complex, Liaoning Province, NE China. *European Journal of Mineralogy*, **24**, 189–196.
- Zhu Y.S., Yang J.H., Sun J.F., Zhang J.H. and Wu F.Y. (2016) Petrogenesis of coeval silica-saturated and silica-undersaturated alkaline rocks: Mineralogical and geochemical evidence from the Saima alkaline complex, NE China. *Journal of Asian Earth Sciences*, **117**, 184–207.
- Zhu Y.S., Yang J.H., Sun J.F. and Wang H. (2017) Zircon Hf–O isotope evidence for recycled oceanic and continental crust in the sources of alkaline rocks. *Geology*, **45**, 407–410.